ADVANCING EARTH AND SPACE SCIENCES

Geophysical Research Letters®

RESEARCH LETTER
10.1029/2024GL113309

Special Collection:
Advances and Best Practices in Boron-based paleo-CO2 reconstruction

Key Points:

- Inverting cloud top XCO_2 using lidar reflection signals above the cloud enhances the utilization of satellite observation data
- Based on passive satellite and model data, the accuracy of atmospheric environment monitoring satellite data inversion is demonstrated
- First use of active remote sensing satellites for assessment of marine carbon uptake

Correspondence to:
L. Bu,
001779@nuist.edu.cn

Citation:
Mao, Z., Zhang, Y., Bu, L., Wang, Q., Xiao, W., Lee, X., et al. (2024). Measurement of CO_2 column concentration above cloud tops with a spaceborne IPDA lidar. *Geophysical Research Letters*, *51*, e2024GL113309. https://doi.org/10.1029/2024GL113309

Received 7 NOV 2024
Accepted 21 NOV 2024

Author Contributions:
Conceptualization: Zhihua Mao, Yang Zhang, Lingbing Bu
Data curation: Yang Zhang, Lingbing Bu, Jiqiao Liu, Weibiao Chen, Sihan Liu, Zhongting Wang
Formal analysis: Zhihua Mao, Dingyuan Liang, Khalid Muhammad Burhan
Funding acquisition: Yang Zhang, Lingbing Bu, Qin Wang, Wei Xiao
Methodology: Zhihua Mao
Project administration: Yang Zhang, Lingbing Bu, Qin Wang, Wei Xiao
Resources: Zhihua Mao, Yang Zhang, Lingbing Bu, Qin Wang, Wei Xiao, Xuhui Lee, Jiqiao Liu, Weibiao Chen, Sihan Liu, Zhongting Wang

Measurement of CO_2 Column Concentration Above Cloud Tops With a Spaceborne IPDA Lidar

Zhihua Mao[1], Yang Zhang[2], Lingbing Bu[1], Qin Wang[3], Wei Xiao[4], Xuhui Lee[5], Dingyuan Liang[6], Khalid Muhammad Burhan[1], Jiqiao Liu[7], Weibiao Chen[7], Sihan Liu[8], and Zhongting Wang[8]

[1]School of Atmospheric Physics, Nanjing University of Information Science and Technology, Nanjing, People's Republic of China, [2]China Aerospace Science and Technology Corp No 8 Academy No 509 Research Institute, Shanghai, People's Republic of China, [3]Tianjin Meteorological Service, Tianjin, People's Republic of China, [4]Nanjing University of Information Science and Technology, Yale-NUIST Center on Atmospheric Environment, Nanjing, People's Republic of China, [5]Yale University, School of the Environment, NewHaven, CT, USA, [6]Division of Environment and Sustainability, The Hong Kong University of Science and Technology, Hong Kong, People's Republic of China, [7]Key Laboratory of Space Laser Communication and Detection Technology, Shanghai Institute of Optics and Fine Mechanics, Chinese Academy of Sciences, Shanghai, People's Republic of China, [8]Satellite Application Center for Ecology and Environment, Ministry of Ecology and Environment, Beijing, People's Republic of China

Abstract The Atmospheric Environment Monitoring Satellite (AEMS), launched by China in 2022, was equipped with active remote sensing lidar for carbon monitoring. It adopts the Integrated Path Differential Absorption (IPDA) technology to monitor global CO_2 column concentration (XCO_2). The calculation of cloud top XCO_2 requires cloud height data. A comparison between SRTM global elevation data and 1,572 nm channel elevation data reveals a coefficient of determination (R^2) of 0.998, with an average deviation of 1.24 m. The cloud top XCO_2 observations are consistent with the OCO-2 and CarbonTracker trends. The ocean carbon uptake rate, assessed by the difference in CO_2 concentration between cloud top and sea surface, is −0.319 mmol/m^2/h, which is in good agreement with the associated carbon flux data. This demonstrates the great potential of IPDA lidar for remote sensing of cloud top CO_2 and quantifying ocean carbon uptake.

Plain Language Summary For global greenhouse gas monitoring, passive remote sensing technology has consistently struggled to balance the reliability and usability of monitoring data in cloudy regions. The AEMS employs 1,572 nm IPDA lidar technology for active remote sensing of global XCO_2, enabling effective processing and utilization of cloud echo data. In this study, we focused on the concentrations of CO_2 columns using cloud top echoes and performed a preliminary comparison of cloud top XCO_2 results with related data products from the passive satellite OCO-2 and CarbonTracker. By quantifying the difference in CO_2 concentration between two altitude layers above the sea surface, we assessed ocean carbon absorption capacity, and the results demonstrated high reliability. This work highlights the significant advantages of spaceborne IPDA lidar in global CO_2 measurement, cloud echo data processing, and ocean carbon flux assessment, providing valuable data support for climate change research.

1. Introduction

CO_2 is the most significant greenhouse gas (GHG) in the atmosphere, contributing approximately 80% to the increase in radiative forcing over the past 5 years (IEA, 2022). The continuous rise in its concentration, primarily driven by human activities, is a key factor in global climate warming. Therefore, high-precision, all-weather, and extensive observations of atmospheric CO_2 concentrations are crucial for advancing carbon reduction efforts, identifying carbon sources and sinks, understanding the carbon cycle, promoting carbon science applications, and supporting global climate change research (Araki et al., 2010; Zhao et al., 2023). Monitoring CO_2 in the lower atmosphere through remote sensing is essential for identifying carbon sources and sinks. Current greenhouse gas monitoring satellites, such as GOSAT, OCO-2, and OCO-3, measure sunlight scattered from the Earth's surface to calculate total column CO_2 content. After decades of development, this technology has become highly accurate. However, passive remote sensing, which relies on sunlight, is limited by solar elevation angles, making it incapable of observations at night and in high-latitude regions. It is also vulnerable to interference from clouds and aerosols, which can obscure slight variations in CO_2 concentration and reduce the reliability of data inversion under cloudy conditions (Chevallier et al., 2014; Liang et al., 2017; Zheng et al., 2023). Approximately two-thirds

Supervision: Zhihua Mao, Yang Zhang, Lingbing Bu, Qin Wang, Wei Xiao, Xuhui Lee, Jiqiao Liu, Weibiao Chen, Sihan Liu, Zhongting Wang
Validation: Zhihua Mao
Writing – original draft: Zhihua Mao
Writing – review & editing: Zhihua Mao

of the Earth's surface is covered by clouds, which further diminishes the effectiveness of passive remote sensing satellite data (Feng et al., 2016). Therefore, compensating for the missing CO_2 information in cloudy regions would significantly enhance the usability of observation data (Baker et al., 2010; Palmer et al., 2019).

In 2007, the U.S. National Research Council proposed the ASCENDS program in its investigative report, which aims to actively detect atmospheric CO_2 emissions during both nighttime and daytime across different seasons (US NRC, 2007). During NASA's ASCENDS airborne experiment activities in 2011, high-resolution measurements of absorption line shapes were conducted using airborne equipment to distinguish echoes from shallow cumulus cloud tops and the ground. This enabled the determination of CO_2 VMR (volume mixing ratio) in the PBL (planetary boundary layer). In subsequent studies, the cloud slicing method was used to derive VMRs for three vertical layers (Ramanathan et al., 2015). The study found that compared to ground-based XCO_2 measurements, the bias in cloud top CO_2 measurements is smaller, but the standard deviation is larger. This is primarily influenced by cloud top roughness and reflectance (Mao et al., 2018). In 2017, the Shanghai Institute of Optics and Fine Mechanics (SIOM) of the Chinese Academy of Sciences conducted a ground-based validation experiment for atmospheric CO_2 measurement using a 1.57 μm IPDA lidar system (Du et al., 2017). Subsequently, SIOM collaborated with NUIST and other institutions to successfully develop a scaled-down airborne version of the spaceborne ACDL system. This system was deployed for airborne CO_2 observation experiments (Zhu et al., 2020). In 2018 and 2021, two airborne calibration flights were conducted in Shanhaiguan, a coastal city, and Dunhuang, a desert region, to demonstrate the feasibility and precision limits of the system and its retrieval algorithms under complex geographical conditions (Fan et al., 2024; Wang et al., 2022). Both ground-based and airborne results indicated that the ACDL prototype could achieve sub-ppm accuracy, providing high-precision CO_2 measurements on a global scale (Wang, Mustafa, et al., 2021; Zhu et al., 2021). In April 2022, China launched the world's first satellite equipped with CO_2 laser detection capabilities: the Atmospheric Environment Monitoring Satellite (AEMS). Its primary payload, the ACDL system, incorporates an IPDA lidar designed for global CO_2 monitoring. AEMS is designed to measure atmospheric CO_2 with a precision of better than 1 ppm, featuring a land resolution of 50 km and an ocean resolution of 100 km. Using the Total Carbon Column Observing Network (TCCON) as the reference for cross-validation, comparisons between AEMS and TCCON XCO_2 observations indicate that ACDL's measurement bias is less than 1 ppm, with a system bias of 0.1 ± 1 ppm (Fan et al., 2024; Zhang et al., 2024). This paper analyzes cloud top echo signals based on ACDL observation data from July 2022, compares spaceborne IPDA lidar cloud top XCO_2 observations with OCO-2 and CarbonTracker product data, and quantifies ocean carbon absorption intensity. The data comparison and application provide a preliminary analysis of the ability of the IPDA lidar to remotely sense cloud top CO_2 column concentrations.

2. Instrumentation and Methods

2.1. ACDL System and IPDA Lidar

The main mission of ACDL is to use active laser technology for all-weather detection of global atmospheric aerosols and cloud vertical profiles, as well as global atmospheric CO_2 concentration. This provides scientific data for air quality monitoring, studying Earth's carbon cycle, and identifying carbon sources and sinks. The spaceborne ACDL system's laser emits four wavelengths: 532 , 1,064, 1,572.024 nm (online), and 1,572.085 nm (offline). The atmospheric CO_2 detection method is the IPDA technique, corresponding to the 1572 nm channel.

2.2. XCO_2 Calculation Methods

The IPDA lidar emits two wavelengths, referred to as the online wavelength and the offline wavelength. As the laser travels along the optical path, the online wavelength is strongly absorbed by CO_2 molecules along the path, while the offline wavelength is only weakly absorbed. By receiving the pulse echo signals of both wavelengths, the CO_2 column concentration along that transmission path is ultimately obtained Figure 1 illustrates the working principle of the spaceborne IPDA lidar system, where XCO_2 can be obtained using Equation 1,

$$XCO_2 = \frac{\tau_{CO_2}}{2 \times 10^{-6} \cdot IWF} \tag{1}$$

where τCO_2 is the differential absorption optical depth (DAOD) and *IWF* denotes the integral weight function (Zhu et al., 2019).

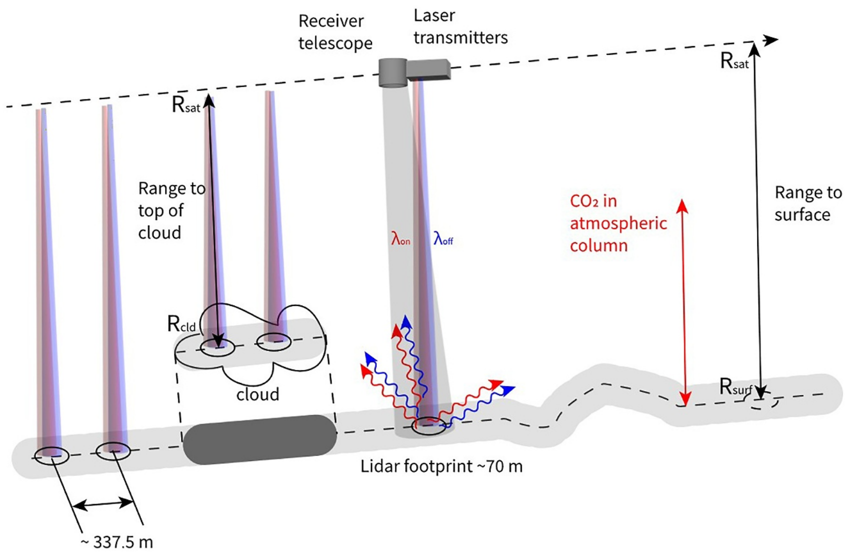

Figure 1. Schematic diagram of spaceborne IPDA lidar principle.

Using the passive satellite OCO-2 and the CarbonTracker (CT) product, it is possible to calculate atmospheric XCO_2 profiles, the results of which can be used for comparison with IPDA lidar cloud top observations. The calculation of the XCO_2 data at the corresponding altitude is represented by Equation 2 (Wunch, D et al., 2010; Mustafa et al., 2020).

$$XCO_2^O = XCO_2^a + \sum_j P_j^T K_j * \left(CO_2^i - CO_{2a}\right) \tag{2}$$

where XCO_2^a is the a priori value of XCO_2, P is the pressure weight function, K is the column averaging kernel, CO_2^i is the CO_2 of the corresponding height stratum of CT, CO_{2a} is the a priori contour value, j is the corresponding vertical height stratum, and T stands for matrix transpose.

2.3. Methods for Calculating Ocean Carbon Fluxes

Observations using cloud top XCO_2 can be used to calculate atmospheric *'XCO_2' b*elow the clouds, and the difference in concentrations can be used to assess changes in carbon fluxes at the subsurface, where in the oceans the carbon uptake can be calculated by Equation 3 (Shi et al., 2021).

$$F_c = \rho w (XCO_{2C} - XCO_{2ABL}) \tag{3}$$

Where F_c is the ocean carbon uptake, ρ is the density of the atmospheric boundary layer, w is the vertical wind speed at the cloud top, and XCO_{2C} and XCO_{2ABL} are the CO_2 column concentrations at the cloud top and boundary layer, respectively.

3. ACDL Cloud Echo Data Analysis and Processing

3.1. Comparison of Altitude Measurement Data

Obtaining accurate cloud top XCO_2 data relies on the precise calculation of the IWF and cloud top pressure, with accurate measurement of cloud top altitude being a key factor (Jacobs et al., 2024). The IPDA lidar system employs a 1,572 nm wavelength in the near-infrared spectrum, achieving sub-meter accuracy in distance measurements (Arnold et al., 2019). This wavelength significantly reduces Rayleigh scattering caused by atmospheric molecules and effectively penetrates atmospheric water vapor, thereby minimizing the impact of atmospheric absorption on measurement precision. Even in the presence of stratus clouds, the system can still attain the necessary accuracy in distance measurements (Gong et al., 2014; Mao et al., 2018; Sharma et al., 2016). The reflectivity of stratus clouds in the 1,572 nm band can be up to 0.05 or even higher, and their surface-hard-target nature can be used as a hard scattering surface for IPDA lidar to obtain accurate cloud top heights (Wang et al., 2020).

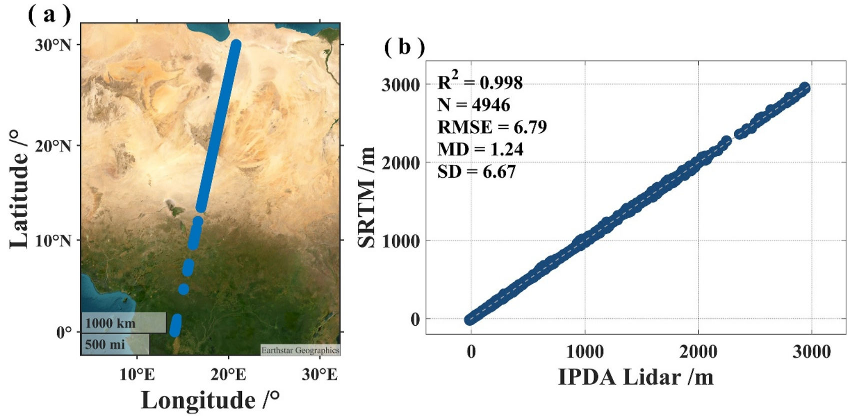

Figure 2. Comparison of ACDL 1572 nm channel altitude measurements with SRTM elevation data.

The Shuttle Radar Topography Mission (SRTM), conducted jointly by NASA and the National Geospatial-Intelligence Agency (NGA), is a global elevation measurement project with a global elevation accuracy of 16 m (90% confidence) (Yang et al., 2011). Figure 2 compares ACDL elevation observation data with SRTM data from a region of the African Sahara Desert with minimal human activity and footprints (discontinuities are due to the exclusion of cloud data). In this area, the root mean square error (RMSE) between ACDL and SRTM data is 6.79 m, the coefficient of determination (R^2) is 0.998, the mean deviation (MD) is approximately 1.24 m, and the standard error (SD) is 6.67 m. These results demonstrate the high reliability of the ACDL system's elevation data.

3.2. Cloud Echoes Data Processing

In the absence of observational equipment with vertical resolution and airborne experiments for comparing cloud top observations, ice crystal particle scattering at higher altitudes in cumulus and cirrus clouds can result in extended optical paths. Significant fluctuations in cumulus cloud top heights and steep gradients of their boundaries can increase observational noise for these cloud types. Additionally, the laser's ability to penetrate most cirrus clouds diminishes detection effectiveness. In contrast, selecting stratus clouds can mitigate the instability of deviations caused by large fluctuations in cloud top height and extended optical paths due to ice crystal particles (Guerlet et al., 2013; Mao et al., 2018, 2024). We use two indicators, echo signal strength and signal-to-noise ratio threshold, to exclude invalid values from different types of echo data.

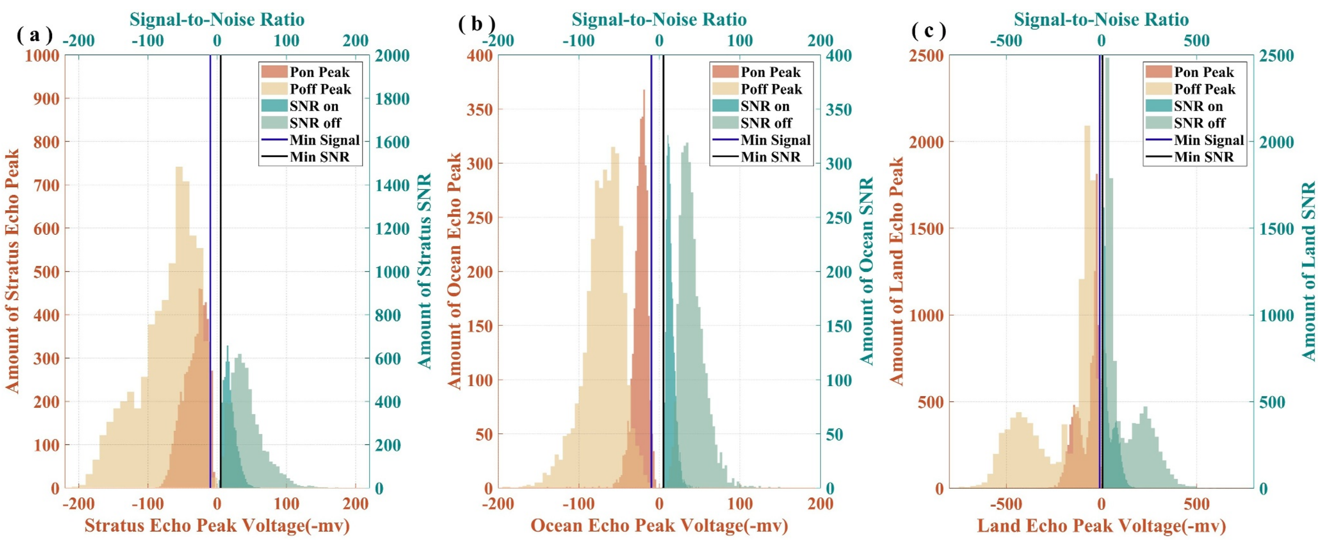

Figure 3. Peak values and signal-to-noise ratio distributions of echo signals for different types of reflective surfaces. (a) Stratus clouds (b) sea surface (c) ground surface.

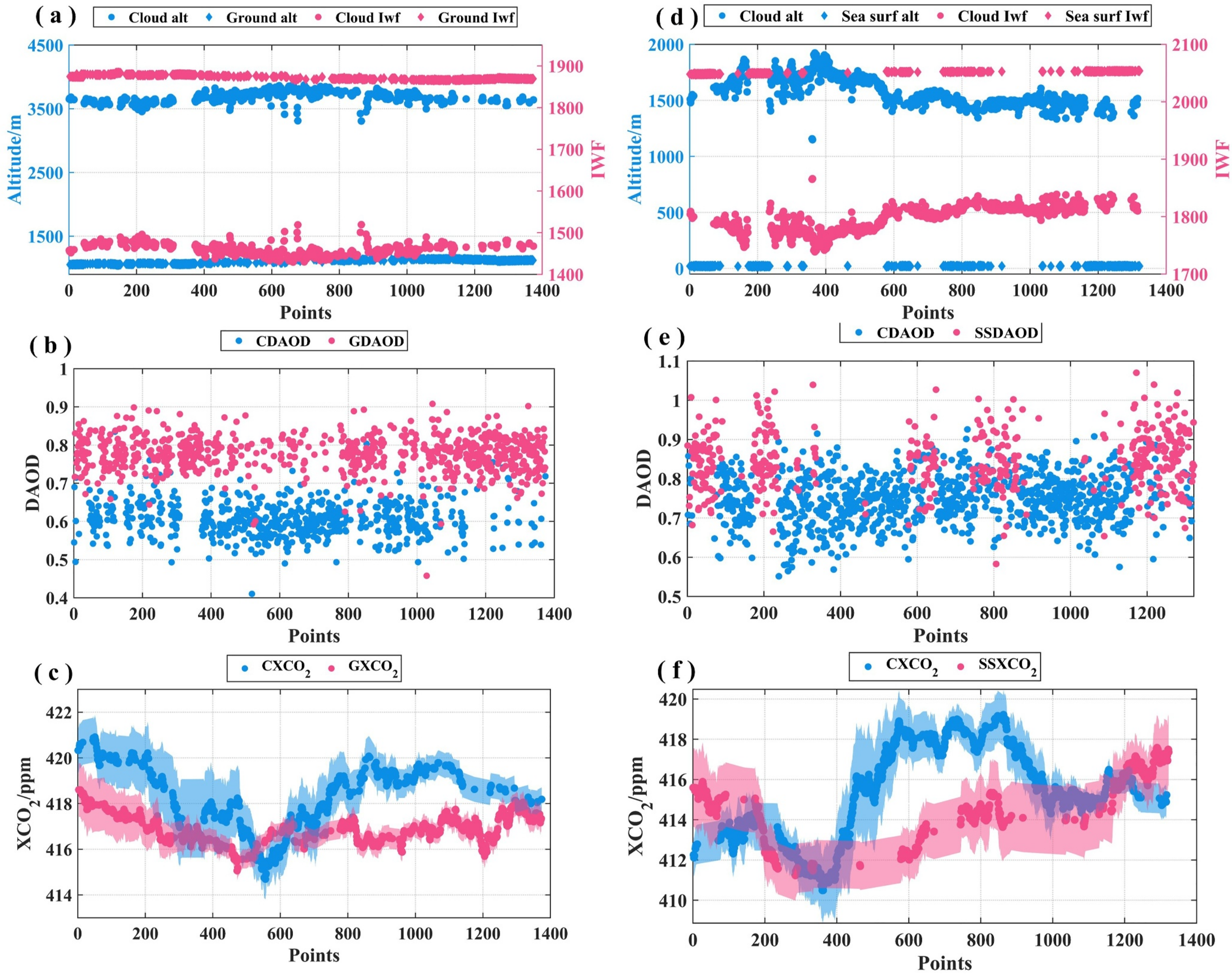

Figure 4. Cloud Top, Ground Surface, and Sea Surface Elevation and IWF, DAOD, XCO_2 Distribution (where the Ground examples are a, b, c, and the Sea examples are d, e, f, with shaded areas representing the standard deviation).

According to the statistical comparison results in Figure 3, 93.4%, 97.4%, and 98.8% of stratus clouds top, sea surface, and surface echo signals, respectively, met the screening criteria. This indicates that the three types of echo data exhibit good spatial and temporal continuity. Among them, the land echo is the strongest, followed by the stratus clouds top, while the sea surface is the weakest. As depicted in Figure 3a, the peak distribution of stratus cloud top echo signal intensity ranges from −24 to −27 mV, with the signal-to-noise ratio peaking between 14 and 16. In comparison, sea surface signal intensity peaks between −18 and −20 mV, with a signal-to-noise ratio of 10–11 (Figure 3b). The echo strength from stratus cloud-tops surpasses that of the sea surface, ranking just below ground surface echoes (Figure 3c). This indicates the high quality of stratus cloud top echo signals and the high value of enhancing the utilization of IPDA lidar cloud top data.

4. Results

4.1. Calculation of Cloud-Top XCO_2

The relative variations in both macro- and micro-meteorological phenomena (e.g., wind, convection, and turbulence) and the spatial distribution of surface carbon sources and sinks contribute to fluctuations in CO_2 concentrations influenced by atmospheric dynamics (Abshire et al., 2014; Fu et al., 2018; Lu et al., 2022; Mao et al., 2024). As shown in Figures 4a and 4d, the cloud top heights are approximately 3,695 m and 1,586 m,

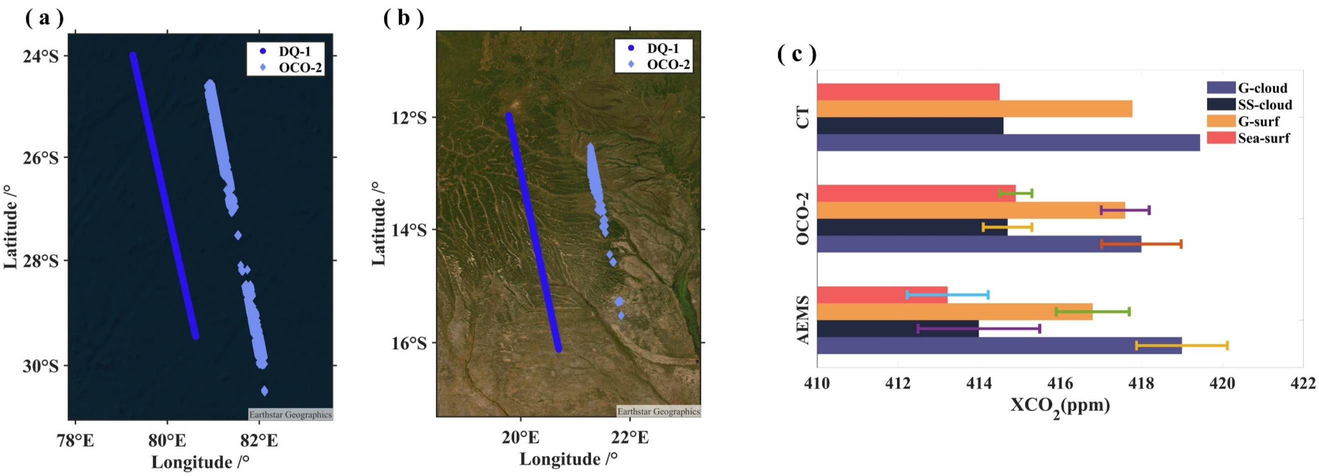

Figure 5. Satellite footprint distribution and vertical observation comparison results.

respectively. The comparison reveals that the cloud top DAOD is smaller, with differences of approximately 0.17 and 0.10. This is due to the higher altitude of the cloud tops compared to the surface and sea level, which reduces the influence of anthropogenic factors and natural emissions. Most CO_2 is concentrated near the surface, leading to higher DAOD from the surface and sea level to the top of the atmosphere compared to that from the cloud top to the top of the atmosphere.

Two of the satellites are about 140 and 165 km apart at their sub-stellar points, as shown in Figure 5. The data from AEMS, OCO-2, and CT exhibit minor differences in the vertical direction, and the trends in vertical variation are consistent, with similar vertical distribution structures. This indicates that the CO_2 concentration distribution in the vertical direction of the atmosphere in this region increases with height. This phenomenon is mainly due to the consumption of CO_2 by daytime terrestrial plant photosynthesis and the absorption of CO_2 by the ocean in the lower atmosphere. Detailed vertical observation comparison results are shown in Table 1. When the signal-to-noise ratio of the cloud top echo is sufficiently high, the accuracy and random error distribution of cloud top XCO2 observations become comparable to those of land echo, exhibiting higher accuracy and reduced random error.

4.2. Assessment of Ocean Carbon Sequestration Capacity

Since the Industrial Revolution, the global oceans have absorbed about 30% of human-emitted CO_2 (Khatiwala et al., 2013). The global oceans' absorption of CO_2 has played a crucial role in mitigating the increase in atmospheric CO_2 levels caused by human activities (Landschützer et al., 2014; Wang, Mustafa, et al., 2021). Furthermore, assessing the amount of CO_2 absorbed by the oceans has always been a key focus and challenge in carbon monitoring. Dang et al. proposed an idealized boundary layer model in 2011 to estimate the regional CO_2 net flux of forests and grasslands. This model has promising applications in regions with minimal human emission interference, such as oceans and forests (Dang et al., 2011). When oceanic XCO_{2ABL} is calculated to be 392 ppm,

Table 1
Comparison of Vertical Observations in Different Data Sets (MRE Represents the Average Random Observation Error, MSNR Stands for Average Echo Signal-To-Noise Ratio)

DataSet	Ground-surf	GS-cloud	Sea-surf	SS-cloud
AEMS	416.8 ± 0.9 ppm	419 ± 1.12 ppm	413.22 ± 1 ppm	413.99 ± 1.5 ppm
	MRE:0.386 ppm (0.096%)	MRE:0.455 ppm (0.11%)	MRE:1.298 ppm (0.32%)	MRE:1.315 ppm (0.33%)
	MSNR:52.8	MSNR:45.9	MSNR:15.5	MSNR:15.8
OCO-2	417.6 ± 0.59 ppm	418 ± 0.98 ppm	414.9 ± 0.4 ppm	414.7 ± 0.6 ppm
CT	417.78 ppm	419.45 ppm	414.5 ppm	414.6 ppm

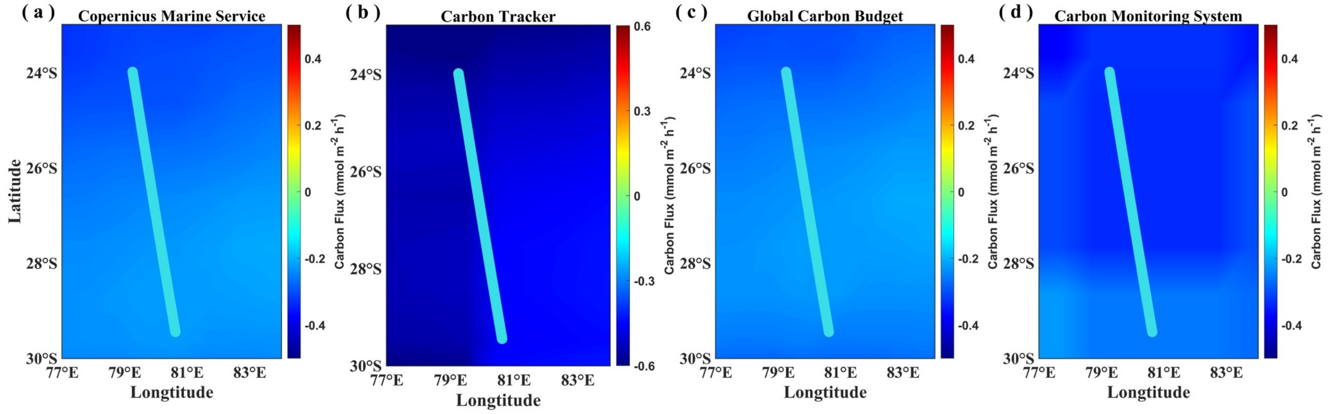

Figure 6. Distribution of ocean carbon absorption.

the oceanic carbon absorption amount for the region is −0.319 mmol/m^2/h as calculated by Equation 3, with a total uncertainty of 7.2%, aligning well with existing ocean carbon flux data.

As shown in Figure 6, the light blue lines represent the footprints of the AEMS satellite. The carbon absorption amounts in this sea area are −0.26, −0. 52, −0.24, and −0.32 mmol/m^2/h (Figure 6a to Figure 6d), respectively. The small differences between the oceanic carbon absorption amounts calculated by the IPDA lidar and the related data indicate the reliability of calculating oceanic carbon absorption through cloud echo differences. The terrestrial environment exhibits a more complex distribution of anthropogenic carbon emission sources, diverse surface types, and ecosystems. Relevant models are currently under development and will be detailed in future publications.

5. Discussion and Conclusions

Due to the high signal-to-noise ratio of the IPDA lidar for certain types of cloud echoes, processing cloud data can significantly enhance the utilization of satellite observation data. In addition, we studied the vertical distribution characteristics of CO_2 based on cloud echoes that can help to identify the carbon sources and sinks in the lower atmosphere and update our dynamic understanding of the carbon cycle.

The IPDA lidar is a highly precise greenhouse gas observation device, but the calculation of the elevation of hard targets is a critical factor that is affecting its accuracy. By comparing with SRTM data, the ACDL elevation data achieve an R^2 of 0.998 with a root mean square error of only 6.67 m. The AEMS cloud top XCO_2 results show small differences from those of passive satellites and models, with similar trends. The oceanic carbon absorption capability was assessed using XCO_2 concentration differences based on cloud echo observations from the spaceborne IPDA lidar and vertical height layers at the sea surface. The results show that the ocean carbon absorption in the region is −0.319 mmol/m^2/h, which is consistent with carbon flux data from GCB, CMS, CT, and CMEMS-LSCE. Future work will involve a detailed analysis of other types of cloud echoes and will use nighttime lidar observation data to estimate diurnal and nocturnal ocean carbon absorption, improving the application of data in scientific research.

Conflict of Interest

The authors declare no conflicts of interest relevant to this study.

Data Availability Statement

SRTM global elevation data can be accessed at https://srtm.csi.cgiar.org/srtmdata/. The CO_2 profile data provided by OCO-2 can be obtained from (OCO-2/OCO-3 Science Team et al., 2020). Vertical wind speed data from ERA5 (Hersbach et al., 2023). Ocean carbon flux data can be obtained from Global Carbon Budget (Hauck et al., 2023), Carbon Monitoring System (Liu & Bowman, 2024), CarbonTracker (Jacobson et al., 2024), and Copernicus Marine Service (Global Ocean Surface Carbon, 2023; Chau, T.-T.-T et al., 2022). The AEMS data used in this study was not publicly available at the time of submission. The data can be requested at https://data.cresda.cn/#/home but is not accessible outside of China. Researchers in China with relevant licenses have free access to satellite data.

Acknowledgments

We would like to thank the Environmental Satellite Application Center of the Ministry of Ecology and Environment for providing the AEMS L2B product data. This research was funded by the National Key Research and Development Program of China (Grant 2020YFA0607501), National Natural Science Foundation of China (Grant 42175145). We appreciate the efforts of NASA, NOAA, ECMWF for the data used in this work. We acknowledge the Global Carbon Project, which is responsible for the Global Carbon Budget and we thank the ocean modeling and fCO2-mapping groups for producing and making available their model and fCO2-product output.

References

Abshire, J. B., Ramanathan, A., Riris, H., Mao, J., Allan, G. R., Hasselbrack, W. E., et al. (2014). Airborne measurements of CO_2 column concentration and range using a pulsed direct-detection IPDA lidar. *Remote Sensing*, *6*(1), 443–469. https://doi.org/10.3390/rs6010443

Araki, M., Morino, I., Machida, T., Sawa, Y., Matsueda, H., Ohyama, H., et al. (2010). CO2 column-averaged volume mixing ratio derived over Tsukuba from measurements by commercial airlines. *Atmospheric Chemistry and Physics*, *10*(16), 7659–7667. https://doi.org/10.5194/acp-10-7659-2010

Arnold, D., Montenbruck, O., Hackel, S., & Sosnica, K. (2019). Satellite laser ranging to low Earth orbiters: Orbit and network validation. *Journal of Geodynamics*, *93*(11), 2315–2334. https://doi.org/10.1007/s00190-018-1140-4

Baker, D. F., Bosch, H., Doney, S. C., O'Brien, D., & Schimel, D. S. (2010). Carbon source/sink information provided by column CO2 measurements from the Orbiting Carbon Observatory. *Atmospheric Chemistry and Physics*, *10*(9), 4145–4165. https://doi.org/10.5194/acp-10-4145-2010

Chau, T. T. T., Gehlen, M., & Chevallier, F. (2022). A seamless ensemble-based reconstruction of surface ocean pCO2 and air–sea CO2 fluxes over the global coastal and open oceans. *Biogeosciences*, *19*(4), 1087–1109. https://doi.org/10.5194/bg-19-1087-2022

Chevallier, F., Palmer, P. I., Feng, L., Boesch, H., O'Dell, C. W., & Bousquet, P. (2014). Toward robust and consistent regional CO2 flux estimates from in situ and spaceborne measurements of atmospheric CO2. *Geophysical Research Letters*, *41*(3), 1065–1070. https://doi.org/10.1002/2013GL058772

Chuncan, F., Cheng, C., Jiqiao, L., Yuan, X., Ke, L., Xiaopeng, Z., et al. (2024). Preliminary analysis of global column-averaged CO2 concentration data from the spaceborne aerosol and carbon dioxide detection lidar onboard AEMS. *Optics Express*, *32*(12), 21870–21886. https://doi.org/10.1364/OE.517736

Chuncan, F., Juxin, Y., Jiqiao, L., Lingbing, B., Qin, W., Chong, W., et al. (2024). Airborne atmospheric carbon dioxide measurement using 1.5 m laser double-pulse IPDA lidar over a desert area. *Applied Optics*, *63*(9), 2121–2131. https://doi.org/10.1364/AO.507905

Dang, X., Lai, C.-T., Hollinger, D. Y., Schauer, A. J., Xiao, J., Munger, J. W., et al. (2011). Combining tower mixing ratio and community model data to estimate regional-scale net ecosystem carbon exchange by boundary layer inversion over four flux towers in the United States. *Journal of Geophysical Research*, *116*(G3), G03036. https://doi.org/10.1029/2010JG001554

Feng, L., Palmer, P. I., Parker, R. J., Deutscher, N. M., Feist, D. G., Kivi, R., et al. (2016). Estimates of European uptake of CO2 inferred from GOSAT XCO2 retrievals: Sensitivity to measurement bias inside and outside Europe. *Atmospheric Chemistry and Physics*, *16*(3), 1289–1302. https://doi.org/10.5194/acp-16-1289-2016

Fu, Z., Gerken, T., Bromley, G., Araujo, A., Bonal, D., Burban, B., et al. (2018). The surface-atmosphere exchange of carbon dioxide in tropical rainforests: Sensitivity to environmental drivers and flux measurement methodology. *Agricultural and Forest Meteorology*, *263*, 292–307. https://doi.org/10.1016/j.agrformet.2018.09.001

Global Ocean Surface Carbon. (2023). E.U. Copernicus marine Service information (CMEMS) [Dataset]. *Marine Data Store (MDS)*. https://doi.org/10.48670/moi-00047. Accessed on 12 June 2024.

Gong, W., Ma, X., Dong, Y., Lin, H., & Li, J. (2014). The use of 1572 nm Mie LiDAR for observation of the optical properties of aerosols over Wuhan, China. *Optics and Laser Technology*, *56*, 52–57. https://doi.org/10.1016/j.optlastec.2013.07.015

Guerlet, S., Butzet, A., Schepers, D., Basu, S., Hasekamp, O. P., Kuze, A., et al. (2013). Impact of aerosol and thin cirrus on retrieving and validating XCO_2 from GOSAT shortwave infrared measurements. *Journal of Geophysical Research: Atmospheres*, *118*(10), 4887–4905. https://doi.org/10.1002/jgrd.50332

Hauck, J., Landschützer, P., Mayot, N., & Jersild, A. (2023). Global carbon Budget 2023, surface ocean fugactiy of CO2 (fCO2) and air-sea CO2 flux of individual global ocean biogechemical models and surface ocean fCO2-based data-products [last access: 12 June, 2024] [Dataset]. *Zenodo*. https://doi.org/10.5281/zenodo.10222484

Hersbach, H., Bell, B., Berrisford, P., Biavati, G., Horányi, A., Muñoz Sabater, J., et al. (2023). ERA5 hourly data on pressure levels from 1940 to present [Dataset]. *Copernicus Climate Change Service (C3S) Climate Data Store (CDS)*. https://doi.org/10.24381/cds.bd0915c6. Accessed on 12 June 2024.

IEA. (2022). *Global energy review: CO2 emissions in 2021*. IEA. Licence: CC BY 4.0 Retrieved from https://www.iea.org/reports/global-energy-review-co2-emissions-in-2021-2

Jacobs, N., O'Dell, C. W., Taylor, T. E., Logan, T. L., Byrne, B., Kiel, M., et al. (2024). The importance of digital elevation model accuracy in XCO2 retrievals: Improving the orbiting carbon observatory 2 atmospheric carbon observations from space version 11 retrieval product. *Atmospheric Measurement Techniques*, *17*, 1375–1401. https://doi.org/10.5194/amt-17-1375-2024

Jacobson, A. R., Schuldt, K. N., Arlyn, A., Miller, J. B., Oda, T., Sourish, B., et al. (2024). CarbonTracker CT-NRT.v2024-1 [Dataset]. *NOAA Global Monitoring Laboratory*. https://doi.org/10.15138/3RE5-3Y28. Accessed on 12 June 2024.

Juan, D., Yadan, Z., Shiguang, L., Junxuan, Z., Yanguang, S., Zang, H., et al. (2017). Double-pulse 1.57 μm integrated path differential absorption lidar ground validation for atmospheric carbon dioxide measurement. *Applied Optics*, *56*(25), 7053–7058. https://doi.org/10.1364/AO.56.007053

Khatiwala, S., Tanhua, T., Mikaloff Fletcher, S., Gerber, M., Doney, S. C., Graven, H. D., et al. (2013). Global ocean storage of anthropogenic carbon. *Biogeosciences*, *10*(4), 2169–2191. https://doi.org/10.5194/bg-10-2169-2013

Landschützer, P., Gruber, N., Bakker, D. C. E., & Schuster, U. (2014). Recent variability of theglobal ocean carbon sink. *Global Biogeochemical Cycles*, *28*(9), 927–949. https://doi.org/10.1002/2014GB004853

Liang, A., Gong, W., Han, G., & Xiang, C. (2017). Comparison of satellite-observed XCO2 from GOSAT, OCO-2, and ground-based TCCON. *Remote Sensing*, *9*(10), 1033. https://doi.org/10.3390/rs9101033

Liu, J., & Bowman, K. (2024). Carbon monitoring system carbon flux ocean L4 V3, Greenbelt, MD, USA [Dataset]. *Goddard Earth Sciences Data and Information Services Center (GES DISC)*. https://doi.org/10.5067/9H6GCQKP28AI 12 June 2024.

Lu, Z., Gao, Y., Li, G., Liu, B., Xu, Y., Tao, C., et al. (2022). The analysis of temperature and air entrainment rate for the turbulence diffusion jet flame of propane and carbon dioxide gas mixture. *Energy*, *254*, 124232. https://doi.org/10.1016/j.energy.2022.124232

Mao, J., Abshire, J. B., Kawa, S. R., Sun, X., & Riris, H. (2024). Airborne lidar measurements of atmospheric CO_2 column concentrations to cloud tops made during the 2017 ASCENDS/ABoVE campaign. *Atmospheric Measurement Techniques*, *17*(3), 1061–1074. https://doi.org/10.5194/amt-17-1061-2024

Mao, J., Ramanathan, A., Abshire, J. B., Kawa, S. R., Riris, H., Allan, G. R., et al. (2018). Measurement of atmospheric CO2 column concentrations to cloud tops with a pulsed multi-wavelength airborne lidar. *Atmospheric Measurement Techniques*, *11*(1), 127–140. https://doi.org/10.5194/amt-11-127-2018

Mustafa, F., Bu, L., Wang, Q., Ali, M. A., Bilal, M., Shahzaman, M., & Qiu, Z. (2020). Multi-year comparison of CO2 concentration from NOAA carbon tracker reanalysis model with data from GOSAT and OCO-2 over Asia. *Remote Sensing*, *12*(15), 2498. https://doi.org/10.3390/rs12152498

OCO-2/OCO-3 Science Team, Payne, V., & Chatterjee, A. (2020). OCO-2 Level 2 geolocated XCO2 retrievals results, physical model, Retrospective Processing V11r, Greenbelt, MD, USA [Dataset]. *Goddard Earth Sciences Data and Information Services Center (GES DISC)*. https://doi.org/10.5067/8Z3QQKHC4R4C. Accessed 12 June 2024.

Palmer, P. I., Wilson, E. L., L. Villanueva, G., Liuzzi, G., Feng, L., DiGregorio, A. J., et al. (2019). Potential improvements in global carbon flux estimates from a network of laser heterodyne radiometer measurements of column carbon dioxide. *Atmospheric Measurement Techniques*, *12*(4), 2579–2594. https://doi.org/10.5194/amt-12-2579-2019

Ramanathan, A. K., Mao, J., Abshire, J. B., & Allan, G. R. (2015). Remote sensing measurements of the CO2 mixing ratio in the planetary boundary layer using cloud slicing with airborne lidar. *Geophysical Research Letters*, *42*(6), 2055–2062. https://doi.org/10.1002/2014GL062749

Sharma, S., Vaishnav, R., Shukla, M. V., Kumar, P., Kumar, P., Thapliyal, P. K., et al. (2016). Evaluation of cloud base height measurements from Ceilometer CL31 and MODIS satellite over Ahmedabad, India. *Atmospheric Measurement Techniques*, *9*(2), 711–719. https://doi.org/10.5194/amt-9-711-2016

Shi, T., Han, G., Ma, X., Gong, W., Chen, W., Liu, J., et al. (2021). Quantifying CO2 uptakes over oceans using LIDAR: A tentative experiment in Bohai Bay. *Geophysical Research Letters*, *48*(9), e2020GL091160. https://doi.org/10.1029/2020GL091160

United States National Research Council. (2007). Earth science and applications from space: National imperatives for the next decade and beyond; 2007. Retrieved from http://www.nap.edu/

Wang, Q., Mustafa, F., Bu, L., Yang, J., Fan, C., Liu, J., & Chen, W. (2022). Monitoring of atmospheric carbon dioxide over a desert site using airborne and ground measurements. *Remote Sensing*, *14*(20), 5224. https://doi.org/10.3390/rs14205224

Wang, Q., Mustafa, F., Bu, L., Zhu, S., Liu, J., & Chen, W. (2021). Atmospheric carbon dioxide measurement from aircraft and comparison with OCO-2 and CarbonTracker model data. *Atmospheric Measurement Techniques*, *14*(10), 6601–6617. https://doi.org/10.5194/amt-14-6601-2021

Wang, S., Ke, J., Chen, S., Zheng, Z., Cheng, C., Tong, B., et al. (2020). Performance evaluation of spaceborne integrated path differential absorption lidar for carbon dioxide detection at 1572 nm. *Remote Sensing*, *12*(16), 2570. https://doi.org/10.3390/rs12162570

Wang, Y., Li, X., Song, J., Li, X., Zhong, G., & Zhang, B. (2021). Carbon sinks and variations of pCO 2 in the Southern Ocean from 1998 to 2018 based on a deep learning approach. *Ieee Journal of Selected Topics in Applied Earth Observations and Remote Sensing*, *14*, 3495–3503. https://doi.org/10.1109/JSTARS.2021.3066552

Wunch, D., Toon, G. C., Wennberg, P. O., Wofsy, S. C., Stephens, B. B., Fischer, M. L., et al. (2010). Calibration of the total carbon column observing network using aircraft profile data. *Atmospheric Measurement Techniques*, *3*(5), 1351–1362. https://doi.org/10.5194/amt-3-1351-2010

Yang, L., Meng, X., & Zhang, X. (2011). SRTM DEM and its application advances. *International Journal of Remote Sensing*, *32*(14), 3875–3896. https://doi.org/10.1080/01431161003786016

Zhang, H., Han, G., Chen, W., Pei, Z., Liu, B., Liu, J., et al. (2024). Validation method for spaceborne IPDA LIDAR XCO2 products via TCCON. *Ieee Journal of Selected Topics in Applied Earth Observations and Remote Sensing*, *17*, 16984–16992. https://doi.org/10.1109/JSTARS.2024.3418028

Zhao, H., Gui, K., Yao, W., Shang, N., Zhang, X., Zhang, X., et al. (2023). Seasonal and diurnal variations in XCO2 characteristics in China as observed by OCO-2/3 satellites: Effects of land cover and local meteorology. *Journal of Geophysical Research: Atmospheres*, *128*(18), e2023JD038841. https://doi.org/10.1029/2023JD038841

Zheng, J., Zhang, H., & Zhang, S. (2023). Comparison of atmospheric carbon dioxide concentrations based on GOSAT, OCO-2 observations and ground-based TCCON data. *Remote Sensing*, *15*(21), 5172. https://doi.org/10.3390/rs15215172

Zhu, Y., Liu, J., Chen, X., Zhu, X., Bi, D., & Chen, W. (2019). Sensitivity analysis and correction algorithms for atmospheric CO2 measurements with 1.57-μm airborne double-pulse IPDA LIDAR. *Optics Express*, *27*(22), 32679–32699. https://doi.org/10.1364/OE.27.032679

Zhu, Y., Yang, J., Chen, X., Zhu, X., Zhang, J., Li, S., et al. (2020). Airborne validation experiment of 1.57-μm double-pulse IPDA LIDAR for atmospheric carbon dioxide measurement. *Remote Sensing*, *12*, 1999. https://doi.org/10.3390/rs12121999

Zhu, Y., Yang, J., Zhang, X., Liu, J., Zhu, X., Zang, H., et al. (2021). Performance improvement of spaceborne carbon dioxide detection IPDA LIDAR using linearty optimized amplifier of photo-detector. *Remote Sensing*, *13*(10), 2007. https://doi.org/10.3390/rs13102007